ELSEVIER

Contents lists available at ScienceDirect

Building and Environment

journal homepage: www.elsevier.com/locate/buildenv





Building occupancy estimation using microwave Doppler radar and wavelet transform

Shekh M.M. Islam ^a, Amy Droitcour ^{b,*}, Ehsan Yavari ^c, Victor M. Lubecke ^d, Olga Boric-Lubecke ^d

- ^a Department of Electrical and Electronic Engineering, University of Dhaka, Dhaka, 1000, Bangladesh
- ^b Adnoviv, Inc, Honolulu, HI, 96822, USA
- ^c Aptiv Services, Carmel, IN, 46032, USA
- ^d Department of Electrical and Computer Engineering, University of Hawaii at Manoa, HI, 96822, USA

ARTICLE INFO

Keywords:
Occupancy estimation
Microwave Doppler radar
Wavelet
Scalogram
Segmentation
Occupant count
Occupancy sensing
Time-frequency methods

ABSTRACT

Room-level occupancy estimation is a critical input for real estate management, including building utilization optimization, energy-efficient building control, building security, and occupant health and well-being. Knowing how many people are using a room at a time can enable businesses to use their real estate, energy and human capital more efficiently, reducing operating expenses as well as carbon footprint. Radar-based occupancy estimation is attractive because it is unobtrusive and does not introduce the privacy issues brought with video imaging-based sensors. In this paper, we present an occupant estimation approach based on continuous wave Doppler radar and wavelet-based signal processing techniques. Theoretical background provides a rational for using a wavelet-based time-frequency approach, and comprehensive simulation and experimental results demonstrate the effectiveness of the proposed approaches on a data set that includes 1–10 occupants. These results indicate that Doppler radar with wavelet-based signal processing may be an effective tool for occupant count in smart building applications.

1. Introduction

Businesses can significantly reduce their real estate and energy expenses by minimizing the amount of space they rent and by more efficiently controlling the environment of their indoor spaces [1]. The number of occupants in each space over time is a key input to optimizing square footage, ventilation, lighting, and cleaning, yet occupancy is rarely measured comprehensively enough to enable data-driven optimization of these parameters. Proactively changing the environment can improve employee's mental health [2–6], physical health, decision-making performance [7] and productivity [8–10]. Moreover, occupancy estimation and detection in commercial and residential buildings can play an important role in security management and emergency evacuations [3] and can enable monitoring of the ability of occupants to maintain physical distance when necessary for safety in a pandemic with the airborne viral transmission.

Residential and commercial buildings account for 40% of the total amount of energy used worldwide [11,14]. Globally 28% of CO_2 emissions are caused by buildings, mostly from climate control (e.g., powering lighting, heating, and cooling) [12]. The key to eliminating waste in climate control systems is to provide heating, cooling, ventilation, and

lighting only when, where, and as much as they are needed, and this requires high-resolution occupancy information [13]. Demand-controlled ventilation (DCV) systems provide the appropriate amount of ventilation based on the estimated number of occupants in each room or zone rather than ventilating at a rate set for the maximum occupancy [13] but are not broadly implemented because of the lack of a cost-effective, privacy-preserving, low-lag, accurate occupant count sensor.

Motion-sensing occupancy sensors, such as those using passive infrared (PIR) and ultrasound (US), are popular for lighting control, although they have significant failure rates when occupants are sedentary [13,15,18]. These systems only detect whether someone is moving in the space, and not the number of people present; therefore, they have very limited application in DCV systems, where they are only useful in single-occupancy rooms, such as private offices. Even in these spaces, they risk underventilation when a sedentary occupant causes a false vacancy signal [19]. Occupancy schedules can be suitable for controlling ventilation in spaces for which occupancy levels change on a predictable basis, such as in some classrooms. Spaces with irregular or unforeseen occupancy fluctuations (such as open offices, meeting rooms, performance venues, lobbies, transient spaces, and retail outlets) need a real-time, accurate estimate of the number of occupants for a DCV

E-mail address: amy.droitcour@adnoviv.com (A. Droitcour).

^{*} Corresponding author.

system to provide the right level of ventilation, maximizing energy savings while maintaining air quality.

Currently, carbon dioxide (CO_2) sensors are the most used method of estimating room occupant count, assuming that the rate of CO_2 generation indoors is proportional to the number of occupants. However, the CO_2 -based DCV market has grown very slowly since 1990. Studies have indicated that there are numerous issues with using CO_2 sensors for ventilation control that need to be addressed, including the accuracy of the sensors, maintenance/calibration requirements, and the sensor lag times [3,16,17,20-24].

Advanced occupant counting sensors that provide a near instantaneous, accurate estimate of the number of people present in a room can enable DCV systems to meet their true potential for energy savings and reliability. Technologies currently available and in development include computer vision systems, doorway sensors using different technologies to detect persons entering or leaving a room, sensors integrated into floor tiles, arrays of time-of-flight sensors in ceiling tiles, and analysis of reflections from WiFi signals. Many people are uncomfortable with the privacy risks of ubiquitous video-based sensors, even if they are designed not to record any images, and this has slowed the uptake of these sensors [23,24]. Doorway sensors are not always accurate at determining whether people are entering or leaving, or mis-count people passing through doorways side-by-side, and errors in count accumulate through the day [25]; they are suitable for determining the flow of people in space but insufficiently accurate for broad use in DCV systems. Systems that require arrays of sensors in the floor or ceiling are expensive and complicated to install, especially in retrofit applications. Received signal strength (RSS) of WiFi signals has been used to measure the number of occupants; however, this method is not accurate if one occupant blocks the sensor's line of sight to another occupant [27]. New technologies and algorithms are necessary to accurately determine occupant number while protecting privacy, at a reasonable installation

A Doppler-radar-based sensor has potential to meet all the needs of an occupant count sensor for ventilation control. This type of sensor has been used for non-contact detection of individual vital signs [28-32, 45–47], and occupancy vs. vacancy [26,27,33], but only recently has it been applied to occupant count. Methods used previously [26,48] with Doppler radar estimated the occupancy based on the strength of the received reflected signal and had similar accuracy challenges as the WiFi RSS method mentioned above. In this work, we show that analysis of the time and frequency content of the signal can increase the robustness of the occupant count with the Doppler radar system. The Wavelet Transform (WT) [34] has shown its efficacy to analyze and extract the characteristics of signals that have non-stationary behavior [35-40] in applications such as radar fall detection. Prior attempts for estimating the number of building occupants from room temperature and CO2 concentration using WT also proved its efficacy [41,42]. However, to the authors' knowledge, none of the work in the literature to date has utilized WT or time-frequency analysis for radar-based occupant count.

A single radar-based motion sensor with the wavelet-based algorithms described in this paper can be used to estimate the number of occupants in a room. This technology can potentially be used to optimize real estate utilization and ventilation rate in DCV HVAC systems, reducing real estate and energy costs while keeping occupants

productive and comfortable. It could also be used to calibrate a predictive model for ventilation control, or to calibrate occupancy models to support building simulation, which can in turn support building and systems design. These radar-based sensors can provide occupant count without the errors introduced by doorway sensors, without the delays and inaccuracies of $\rm CO_2$ sensors, without the privacy issues introduced by video-based sensors, and without the high up-front cost of systems that require a dense array of sensors.

In this paper, Doppler radar detection and count of multiple occupants is described theoretically, explaining the spectrum broadening that occurs with increasing numbers of occupants. Wavelet time-frequency analysis using the Morlet wavelet transform and maximum wavelet coefficient frequency (MWCF) and wavelet coefficient energy (WCE) is proposed for occupant estimation. A comprehensive simulation and experimental results demonstrate that MWCF and WCE parameters increase monotonically with the number of occupants. Data analysis with varying wavelet effective support and Doppler radar data window size demonstrate robustness and potential for near real-time implementation of this approach.

2. Theory and simulation

2.1. Microwave Doppler radar detection of respiration of multiple occupants

A microwave Doppler radar transmits an electromagnetic signal; when the signal reflects off objects in the room, it has a phase shift proportional to the motion of those objects and a magnitude proportional to the radar cross section of those objects. If a stationary person is present, the phase shift of the reflected signal is proportional to the tiny movement of the chest surface due to cardiorespiratory activity [43,44]. The phase shift from an occupant can be described as:

$$\theta_1(t) \propto \frac{4\pi}{\lambda} d_1(t) \tag{1}$$

where λ is the wavelength of the transmitted signal and $d_1(t)$ represents a single occupant's chest displacement due to heartbeat and respiration.

Mixers used in radio and radar receivers are inherently nonlinear, and therefore generate intermodulation and harmonic responses [49]. In Doppler radar physiological sensing of multiple stationary occupants, the fundamental tones are those proportional to chest surface motion due to cardio-respiratory activity of each occupant. The intermodulation generates signals at sums and differences of various combinations of multiples of these frequencies, effectively broadening the signal's spectrum at the mixer output.

For simplicity, we will take the case of two occupants to describe how the intermodulation term is theoretically generated [49]. A mixer has two input ports; the reflected signals are applied to the mixer's RF port. Each reflected signal has a carrier frequency f_c and its phase modulated $\theta(t)$. In a continuous wave, direct conversion radar transceiver, the local oscillator (LO) is derived from the transmitted radar signal at frequency f_c , and is applied to the mixer's LO port. An ideal mixer would multiply the RF port signals by the LO port signal, generating sum and difference frequencies. In the case of two occupants, the ideal mixer is acting on two summed RF input signals, generating an output M_2 occupants(t):

$$M_{2 \ occupants}(t) = \cos(2\pi f_{c}t) \\
* \left[A_{1}(t)\cos\left(2\pi f_{c}t + \frac{2\pi}{\lambda}\left(2d_{0,1} + 2d_{1}(t)\right)\right) + A_{2} (t)\cos\left(2\pi f_{c} t + \frac{2\pi}{\lambda}\left(2d_{0,2} + 2d_{2}(t)\right)\right) \right] = \frac{A_{1}(t)}{2} \left[\cos\left[\frac{2\pi}{\lambda}\left(2d_{0,1} + 2d_{1}(t)\right)\right] + \cos\left[4\pi f_{c}t + \frac{2\pi}{\lambda}\left(2d_{0,1} + 2d_{1}(t)\right)\right] \right] \\
+ \frac{A_{2}(t)}{2} \left[\cos\left[\frac{2\pi}{\lambda}\left(2d_{0,2} + 2d_{2}(t)\right)\right] + \cos\left[4\pi f_{c}t + \frac{2\pi}{\lambda}\left(2d_{0,2} + 2d_{2}(t)\right)\right] \right]$$
(2)

Where f_c is the carrier frequency, $A_n(t)$ is the amplitude modulation on the signal reflected by occupant n, $d_{0,n}$ is the distance to occupant n, and $d_n(t)$ is occupant n's time-varying physiological displacement. The output of the mixer consists of modulated components at the sum and difference frequencies. The sum frequency is easily rejected by a lowpass filter, leaving only the difference frequencies, which are at baseband and shown as $B_{2 \ occupants}(t)$:

$$B_{2 \text{ occupants}}(t) = \frac{A_1(t)}{2} \left[\cos \left[\frac{2\pi}{\lambda} \left(2d_{0,1} + 2d_1(t) \right) \right] \right] + \frac{A_2(t)}{2} \left[\cos \left[\frac{2\pi}{\lambda} \left(2d_{0,2} + 2d_2(t) \right) \right] \right]$$
(3)

However, in practice, a mixer is a nonideal multiplier, and in addition to the sum and difference frequencies, it generates harmonics and mixing products other than the desired outputs. The use of a nonideal multiplier can be illustrated by describing the current/voltage (I/V) characteristics of the nonlinear device (the mixer) via a power series,

$$I = a_0 + a_1 V + a_2 V^2 + a_3 V^3 + \cdots$$
 (4)

and letting V equal the sum of the two inputs to the mixer and I equal the mixer output current.

In the case of two breathing occupants,

analytically generating them here.

In radar measurement of physiological motion, the largest signal is respiration, and amplitude modulation $A_n(t)$ is minimal and can be estimated as a constant A_n . Simplifying the phase modulation to include only the respiratory signal, and simplifying the respiratory signal to a cosine, occupant n's physiological motion can be estimated as

$$d_n(t) = \cos(2\pi f_n t) \tag{8}$$

where f_n is occupant n's breathing frequency.

With a direct conversion radar, the DC phase shift $d_{0,n}$ can be removed in hardware or software. It also can be assumed that the voltage of the modulated input signal is much smaller than that of the LO. With these simplifications, and after an appreciable amount of algebraic and trigonometric manipulations, when two occupants are present with breathing frequencies f_1 and f_2 , the mixer output current contains small-signal components at the frequencies:

$$f_{a,b} = af_1 + bf_2$$
, where, $a, b = 0, +1, -1, +2, -2, ...$ (9)

Frequencies other than the fundamental respiratory frequencies are harmonics (where one of a or b is equal to 0 and the other is greater than 1) and intermodulation tones (where both a and b are non-zero). The order of the intermodulation is calculated by a+b. For example, if there

$$V = \cos(2\pi f_c t) + A_1(t)\cos\left(2\pi f_c t + \frac{2\pi}{\lambda}\left(2d_{0,1} + 2d_1(t)\right)\right) + A_2(t)\cos\left(2\pi f_c t + \frac{2\pi}{\lambda}\left(2d_{0,2} + 2d_2(t)\right)\right)$$
(5)

where the first term is the local oscillator, the second term is the reflection from the first occupant, and the third term is the reflection from the second occupant. When this is input to equation (4), the first term, a_0 , is a DC offset, and the second term, a_1V , leaves the signals at the RF frequency which are typically removed by the lowpass filter. The third term, where the voltage is squared, generates a DC offset, the terms where the LO is multiplied by each input, and introduces intermodulation where the signals from the two occupants are multiplied together. With all the DC values lumped together, the baseband signal after lowpass filtering is:

is a presence of two subjects at a breathing rate of $f_1 = 0.25$ Hz and $f_2 = 0.3$ Hz, then a second order intermodulation tone $f_1 + f_2$ will be at 0.55 Hz. The intermodulation products are theoretically infinite, because there are no bounds on a or b, but in practice, the amplitude of intermodulation products decreases with increasing order [49].

As the number of occupants increases, there are more signals that intermodulate (f_1, f_2, \ldots, f_N) with N being the number of occupants present). For example with N occupants present, intermodulation products occur at:

$$I_{BB,squared\ term} = DC + A_1(t) cos \left(\frac{2\pi}{\lambda} \left(2d_{0,1} + 2d_1(t)\right)\right) + A_2(t) cos \left(\frac{2\pi}{\lambda} \left(2d_{0,2} + 2d_2(t)\right)\right) + A_1(t)A_2(t) cos \left(\frac{2\pi}{\lambda} \left(2d_{0,1} + 2d_1(t)\right)\right) cos \left(\frac{2\pi}{\lambda} \left(2d_{0,2} + 2d_2(t)\right)\right)$$
(6)

The last term is the intermodulation term

$$f_{a_1,a_2,a_3,...a_N} = a_1 f_1 + a_2 f_2 + a_3 f_3 + ... + a_N f_N \text{ where, } a_1,a_2,a_3,...,a_N$$

= 0, +1, -1, +2, -2, ... (10)

$$I_{intermodulation} = \frac{A_1(t)A_2(t)}{2} \left(\cos \left(\frac{2\pi}{\lambda} \left(2d_{0,1} + 2d_{0,2} + 2d_1(t) + 2d_2(t) \right) \right) + \cos \left(\frac{2\pi}{\lambda} \left(2d_{0,1} - 2d_{0,2} + 2d_1(t) - 2d_2(t) \right) \right) \right)$$
(7)

where the sum and difference of the respiratory terms occur inside the cosine, spreading the output spectrum. When higher order intermodulation terms are included, the intermodulation terms get more complex, and as such are generated the simulation in the next section rather than

and the order of intermodulation is the sum of coefficients a_x .

When more occupants are present, more high-frequency content is included in the baseband signal, and the baseband signal frequencies are spread more broadly. By analyzing the time-frequency content of the baseband signal to quantify the amount of higher frequency content

and/or the degree of spectrum spreading, the number of occupants can be estimated.

2.2. Wavelet-based time-frequency analysis

The wavelet transform (WT) is suitable for analyzing non-stationary signals that change in frequency and time [34–37]. Radar-based occupancy sensing in realistic environments involves the detection of multiple people, and the resulting signals include multiple fundamental respiratory frequencies as well as signals at mixtures of these frequencies, such as $f_1+f_2,f_1-f_2,2f_2+f_1$, and so on. This signal behavior makes the WT a good choice for analyzing the signal in time-frequency space.

The continuous WT of a signal x(t) is defined as [34,50]:

$$x(\tau, a) = \frac{1}{\sqrt{a}} \int x(t) f^* \left(\frac{t - \tau}{a}\right) dt \tag{11}$$

where x(t) is the time series signal being processed, τ ($\tau > 0$) is a shift factor, a is a scaling factor, and $f^*(\frac{t-\tau}{a})$ is the daughter wavelet which is a scaled and shifted version of the mother wavelet f(t). The basic idea behind the WT is that the mother wavelet is scaled by a, which changes the center frequency, and shifted in time along x(t) by τ to form a daughter wavelet $f(\frac{t-\tau}{a})$. The similarity of the daughter wavelet to x(t) is computed and recorded as the wavelet coefficient corresponding at a and τ . By repeating the above steps for all a and τ until the whole timeseries signal and all frequencies of the interests are covered, we obtain a coefficient matrix [34,50]. This approach not only provides spectral information through scaling but also provides the time domain information via shifting the wavelet across the signal. Each wavelet coefficient represents the amplitude of the signal with scaling factor a, which can be converted to frequency, and shift τ , which can be used to identify the time.

In general, the continuous wavelet transform provides excellent time

resolution for higher-frequency high-order intermodulation products and good frequency resolution for slower events such as single occupant respiration. In physiological processing, the Morlet wavelet is commonly used because its multiple, evenly spaced maxima effectively enable time and frequency localization of periodic physiologic signals [35–39]. This is also important to identify the frequency content of high order intermodulation products from signals with many occupants, as well as the sub-Hertz frequency content of individual respiratory signals.

The Morlet wavelet has a simple numerical implementation, $e^{-\frac{x^2}{2}}\cos(5x)$, which corresponds to about 4 cycles of a sinusoidal signal with its amplitude windowed by a Gaussian function. The Morlet wavelet has what is known as "effective support," which represents the non-zero interval of the mother wavelet. The default effective support of the Morlet wavelet is $[-4\ 4]$. However, the effective support can be changed to adjust the lower and upper limits of the integral. The fundamental frequency in the spectrum is around 0.8 Hz when the effective support is at the default setting of 8 ($[-4\ 4]$). When the effective support is increased to $16([-8\ 8])$, then the spectrum broadens and the fundamental frequency increases to around 1.6 Hz.

In this work, two wavelet parameters, the Maximum Wavelet Coefficient Frequency (MWCF) and Wavelet Coefficient Energy (WCE), are analyzed for their potential to estimate the number of occupants. When the wavelet transform is performed, a two-dimensional set of coefficients is generated, each representing the amplitude of the signal at a specific frequency and point in time. The maximum wavelet coefficient is identified, and the frequency associated with this coefficient is the MWCF. This parameter, sometimes referred to as the "vibrational frequency," has been used for finding resonant frequencies in the fields of geophysics, biomechanics, seismology, and others [57], and seems promising for quantifying spreading of the spectrum time-frequency data. Wavelet Coefficient Energy (WCE) is the other approach explored here to estimate the number of occupants. Like calculation of MWCF, the two-dimensional set of wavelet coefficients, each representing the complex amplitude of the signal at a specific frequency and

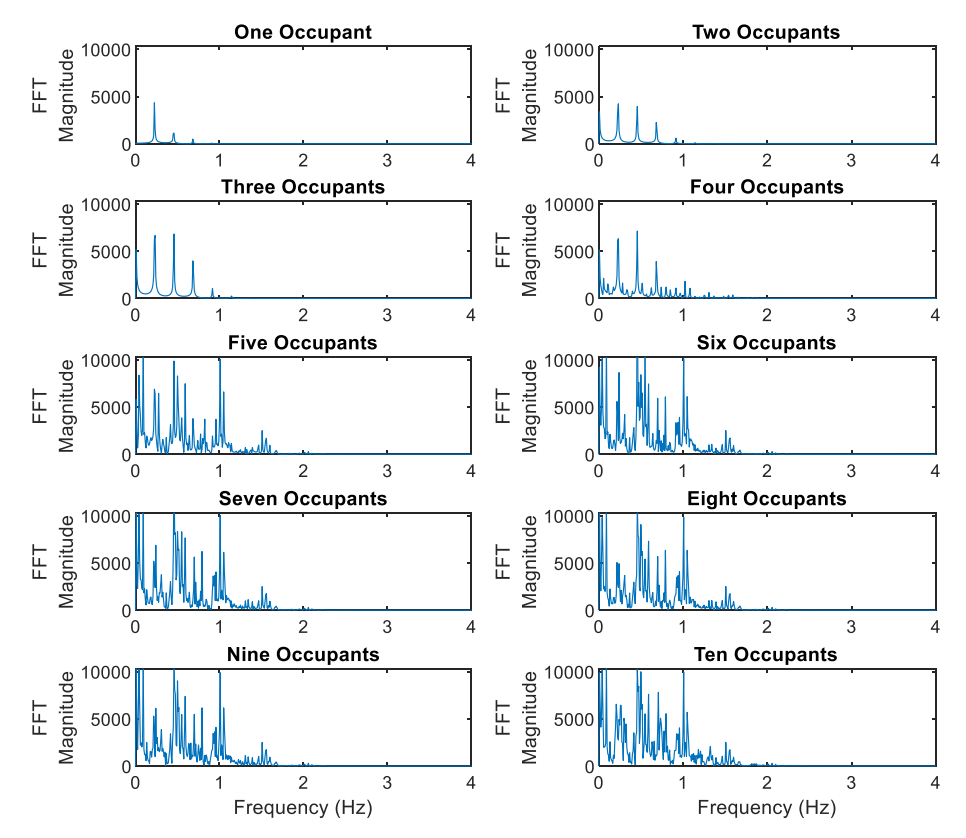


Fig. 1. Frequency spectra of the simulated signal with one to ten occupants. The spectrum broadens as the number of occupants increases.

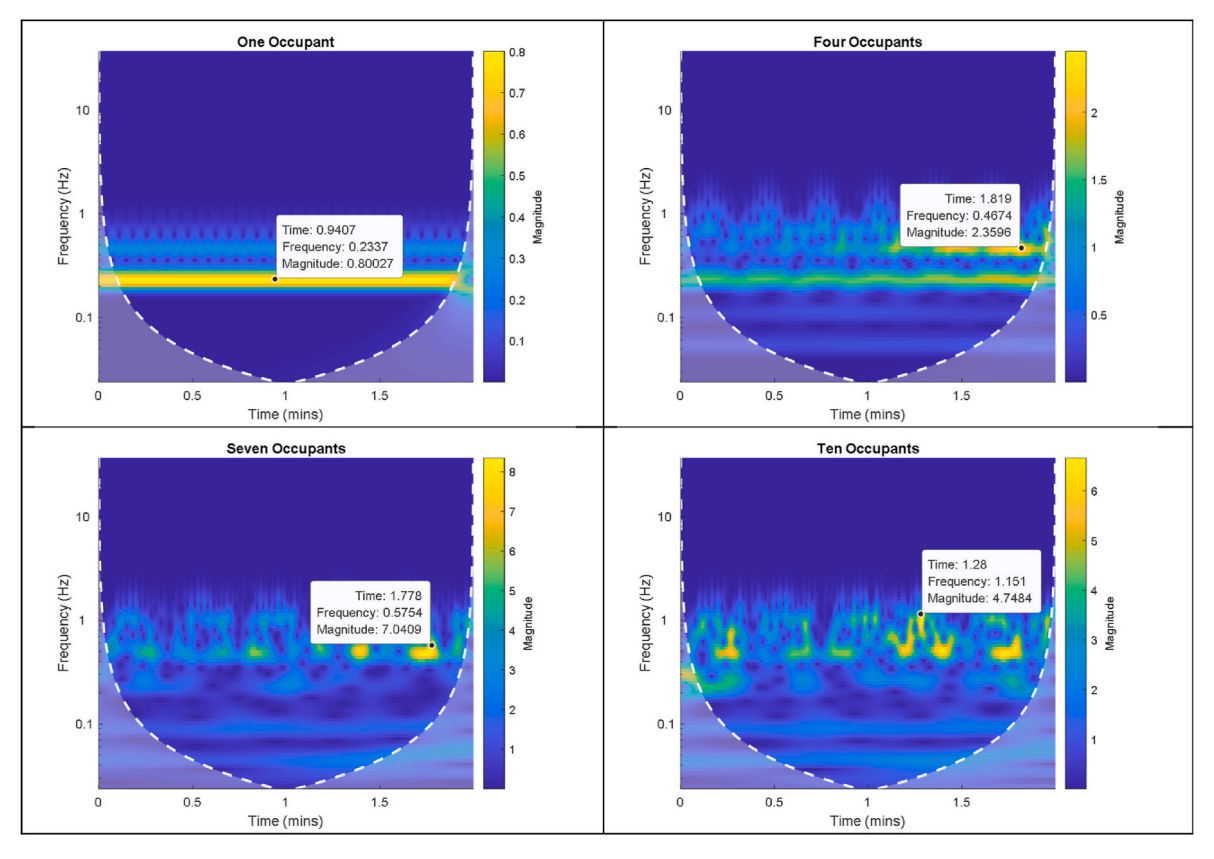


Fig. 2. Wavelet scalogram of the subsampled, lowpass filtered baseband signal from a simulation for (a) one occupant, (b) four occupants, (c) seven occupants, and (d) ten occupants. The spectrum has more variation in both time and frequency as the number of occupants increases, and the frequency associated with the maximum value in time-frequency space also increases with the number of occupants with values of 0.23Hz for one occupant, 0.46Hz for 4 occupants, 0.58Hz for 7 occupants, and 1.2Hz for 10 occupants.

point in time, is used to calculate WCE. The magnitude of the complex amplitude of each wavelet coefficient is squared, and these squared values are summed across the different points in time, and then the square root taken, giving the energy at each frequency. Then the mean of the energy at each frequency is taken as the WCE, or the energy of the signal from the wavelet coefficients, with units of Joules. This approach has been used in other fields, including EEG signal analysis [51,52] and mechanical fault detection [53]. In the following sections, we explore the WCE and MWCF as methods to quantify the spectral spreading, which is expected to increase with increasing numbers of occupants.

2.3. Modelling of occupancy estimation

To better understand the time-frequency content caused by intermodulation of signals from a radar sensor detecting breathing from multiple occupants, a MATLAB simulation was developed. For each simulation run, ten sinusoidal signals were generated at different frequencies within the range of the respiration signals (random values uniformly distributed from 0.2 to 0.3 Hz), with respiratory amplitude randomized from 0.01 to 0.03 m peak to peak. A radio frequency signal (RF) and local oscillator signal (LO) were generated in MATLAB, each as a sinusoidal tone. Because each occupant in a room reflects an RF signal with its phase modulated at the respiratory frequency, a reflected RF signal was generated for each simulated occupant. The simulated received RF signal was the original radio frequency (RF) signal with amplitude randomized from 0.2 to 2, with the phase of the signal having $\,$ an offset randomized from 0 to 2π and an additional phase component with a cosine at the simulated respiratory frequency and amplitude. To simulate a realistic mixer (with nonlinear characteristics) operating on the RF and LO signals, the combined RF signal was summed with the LO

and the combined signal was input into a trinomial equation $y=a_1x+a_2x^2+a_3x^3$. Coefficients used were $a_1=1$, $a_2=1$, and $a_3=0.41$, chosen to simulate a passive diode mixer. The output signals were filtered with a 100-order 25-Hz lowpass FIR filter for anti-aliasing and then downsampled to 100Hz.

Then we performed the fast Fourier transform (FFT) and wavelet transform (WT) using the Morlet wavelet and an effective support of 16 (-8 to 8) of output signals to extract the time-frequency information. Fig. 1 illustrates an example of the FFT outputs in a simulation from one to ten occupants, and the scalograms for a subset of the numbers of occupants is shown in Fig. 2, both from a simulated case where the 10 randomly generated frequencies were: 0.2272 Hz, 0.2291 Hz, 0.2290 Hz, 0.2839 Hz, 0.2742 Hz, 0.2424 Hz, 0.2343 Hz, 0.2203 Hz, 0.2006 Hz, and 0.2493 Hz. The FFT for a single occupant shows the fundamental breathing signal and its harmonics. For increasing numbers of occupants, the spectrum broadens and there is frequency content at frequencies other than the fundamental signals and harmonics from each occupant; this is showing the effects of intermodulation. In Fig. 2, the maximum values in the scalogram are highlighted - these indicate the maximum wavelet coefficient, and the frequency associated with this coefficient is the MWCF (maximum wavelet coefficient frequency). This value increases with the number of occupants present with values of 0.23Hz for one occupant, 0.46Hz for 4 occupants, 0.58Hz for 7 occupants, and 1.2Hz for 10 occupants.

The simulation was then run 1000 times, with different random values for respiratory frequency, respiratory amplitude, received RF amplitude, and phase offset generated each time. For each run, the output for one through ten occupants was generated, the wavelet transform was performed using the Morlet wavelet and an effective support of [–8 8]. The frequency associated with wavelet coefficient

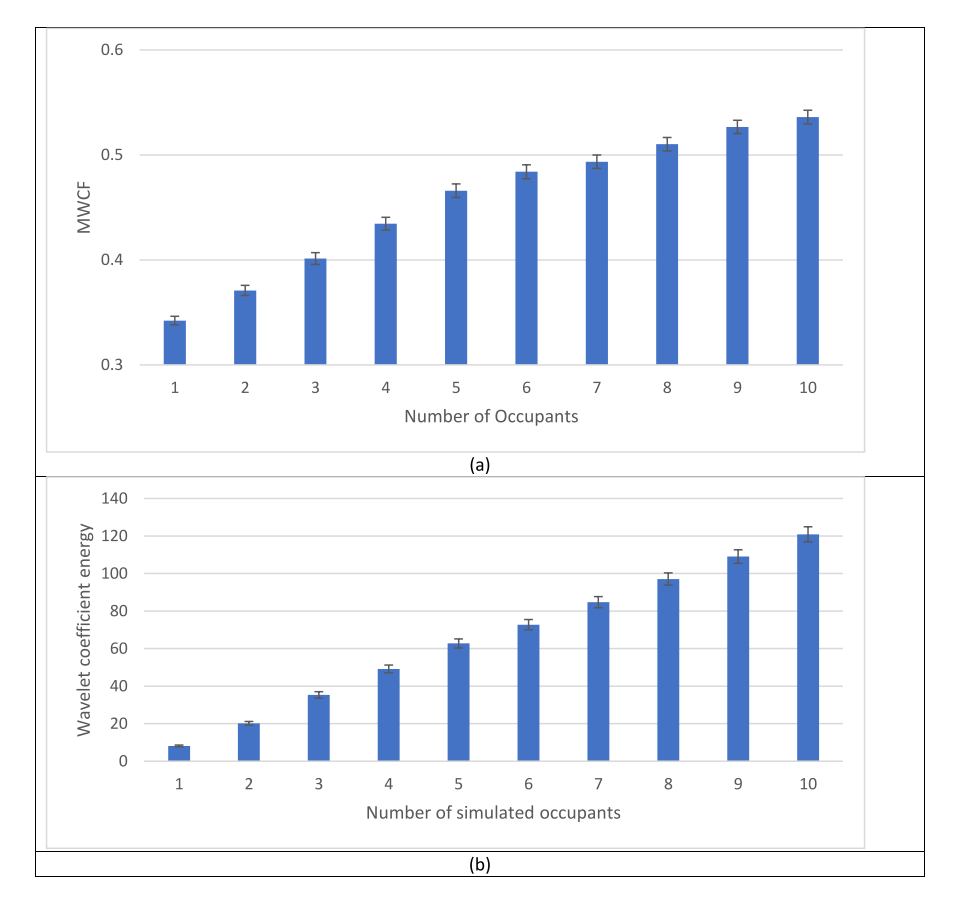


Fig. 3. Relationship between output parameters and the number of occupants when a simulation of Doppler radar signals was generated for one to ten occupants 1000 times. The bars indicate the mean value of the parameter and the standard error of the mean is shown with error bars. a) Relationship between the mean of the maximum wavelet coefficient function (MWCF) and the number of simulated occupants. b. Relationship between the mean of the wavelet coefficient energy (WCE) and the number of simulated occupants. The simulation indicates that with an increase in the number of occupants both the MWCF and WCE tend to increase, and both parameters have potential for determining the number of occupants in a room from a Doppler radar occupancy sensor.

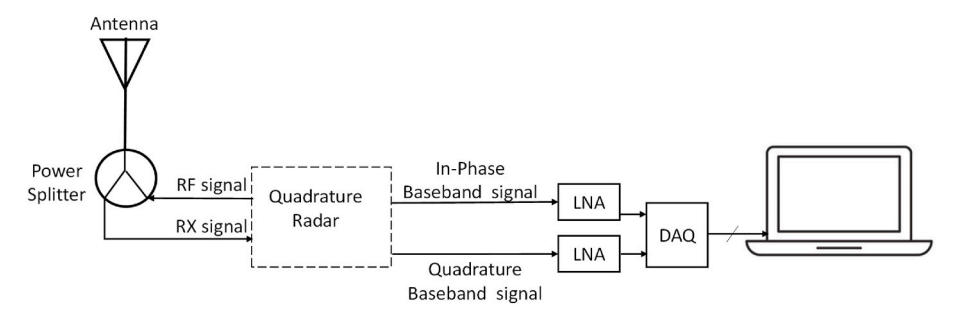


Fig. 4. Block diagram of the experimental hardware setup. The quadrature radar output a RF signal, which was transmitted by the Antenna. The received (RX) signal is returned to the Quadrature Radar where it is split and mixed with the local oscillator signals to generate a quadrature baseband signal, which is filtered and amplified by low noise amplifiers (LNA) before being digitized by the data acquisition system (DAQ) and further processed on a personal computer.

with the greatest amplitude was determined to be the MWCF. The magnitude of each wavelet coefficient was squared, the squares were summed, and the square root was taken to give the energy at each wavelet decomposition; these values were averaged, and the value was determined to be the wavelet coefficient energy (WCE). Then the 1000 MWCF values and the 1000 WCE values identified for each number of occupants were averaged to determine a mean value for each, and the standard error of the mean was determined by calculating the population standard deviation and dividing by the square root of the number of simulations. Fig. 3 shows the mean MWCF (a) and the WCE (b) for each number of occupants when the simulation was run 1000 times, with error bars indicating the standard error of the mean. On average, both the MWCF and the WCE monotonically increase with the number of simulated occupants, and therefore both are potentially suitable for estimating occupant count.

3. Materials and methods

3.1. Hardware prototype

A custom 2.4 GHz Doppler radar with a quadrature receiver, as illustrated in Fig. 4, was used. Agilent E4433B signal generator provided a 2.4 GHz continuous wave signal, split (Mini-Circuits ZFSC 2–250) between the receiver local oscillator (LO) and the transmit antenna (Antenna Specialists ASPPT 2998). Transmit power at the antenna connector is about 7 dBm, resulting in effective isotropic radiated power of about 15dBm with the antenna gain of 8 dBi. A 90-degree power splitter (Mini-Circuits ZX10Q-2-27) is used to drive each passive diode mixer (Mini-Circuits ZFM-4212+) with a 4dBm LO. The backscattered signal received by the antenna is split (Mini-Circuits ZFSC 2–250) between RF ports of two mixers. The mixers down-convert the received RF signals to baseband signals, which are filtered and amplified with Stanford Research amplifiers SR560 with a gain of 200, and bandpass



Fig. 5. Field testing setup for experiment: participants sitting in a relaxed position (people replaced with solid color sketches). (For interpretation of the references to color in this figure legend, the reader is referred to the Web version of this article.)

filters cutoffs at 0.03Hz and 30Hz, and then digitized and recorded.

3.2. Experimental setup

The quadrature radar system described in the previous section was tested in a controlled experiment in a 257 ft² classroom occupied with zero to ten participants. Experiments for this study were conducted according to the Committee on Human Studies (CHS) protocol number 14884, which was approved by the CHS of the University of Hawaii system. All participants provided written informed consent to take part in the study. In the classroom, the first row of seats was 1.5 m away from the antenna, the second row of seats was 3 m away, and the third row of seats was 4.6 m away. The antenna was mounted 2.75 m above the floor, at an angle of 60° from the floor and directed towards the middle of the classroom. The experiment begins with one subject sitting in the front

row, next to the wall and every 90 s, an additional occupant enters the room and walks to a seat every 90 s until 10 occupants were in the room (Fig. 5), and then occupants left the room one by one, every 90 s, until the room was empty [48]. The occupants were instructed to sit still and breathe normally while in their seats. The radar baseband output was recorded for a total of 23 min to complete the experiment.

3.3. Methodology

After data acquisition, the signal was digitally filtered with a 1000 order lowpass FIR filter with a 20 Hz cut-off. Because the physiological signal bandwidth is primarily in the 0-5 Hz band [43], this filter preserves physiological information and respiration intermodulation products, while eliminating high-frequency noise. When a person is walking or making a major movement, there is a much larger reflection. and therefore a larger received signal. In this work, these motions are discarded by comparing the amplitude of the received signal to a threshold and discarding signals that exceed the threshold. Selecting a segment of the signal that does not include large, non-periodic motion, is referred to as segmentation [54]. Segmentation was performed with a threshold of 30% of the maximum signal amplitude to identify and eliminate high-amplitude signals [54]. After segmentation, a 60 s window was used for analysis unless otherwise specified. This segmented, windowed signal was linearly demodulated to extract the phase information. Linear demodulation is a technique in which eigenvalue decomposition is employed to find the maximum displacement information, and the quadrature signals are projected on this vector [55,56]. The continuous wavelet transform was performed with the analytic Morlet wavelet. The highest amplitude wavelet coefficient was identified, and the frequency associated with this wavelet coefficient - the maximum wavelet coefficient frequency, or MWCF -and the energy of the wavelet coefficients - the wavelet coefficient energy, or WCE - were compared with room occupancy.

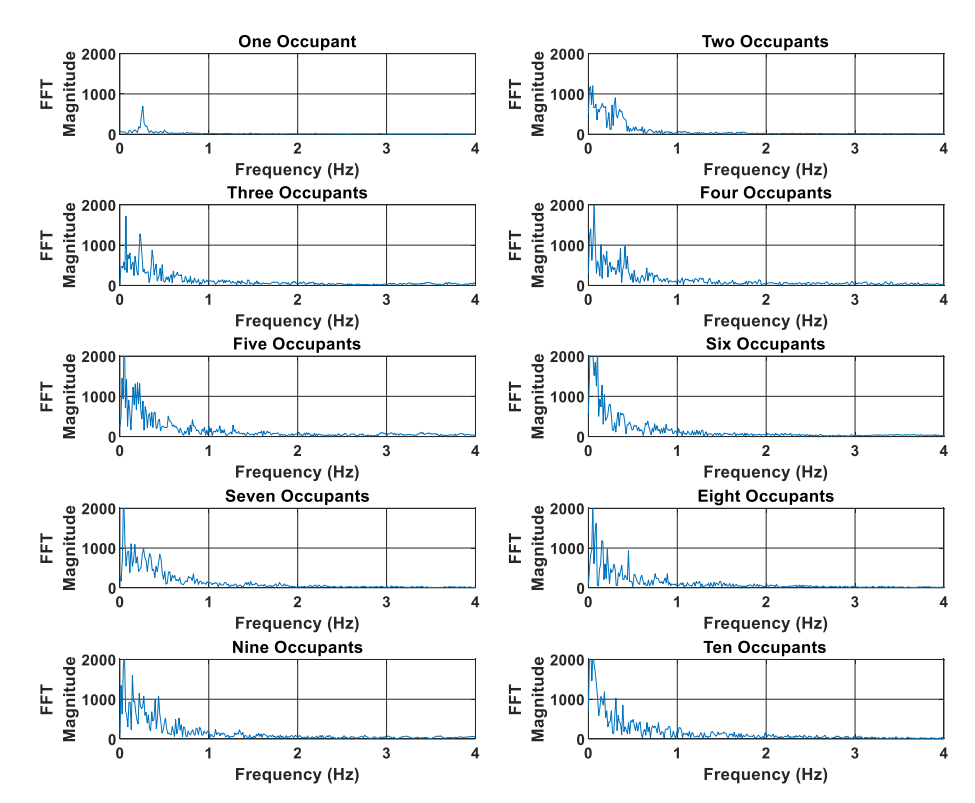


Fig. 6. The FFTs of experimental radar signals from one through ten occupants. The data from a single occupant shows a peak at the breathing frequency, and there is significant spectrum broadening as the number of occupants increases, similar to the simulation.

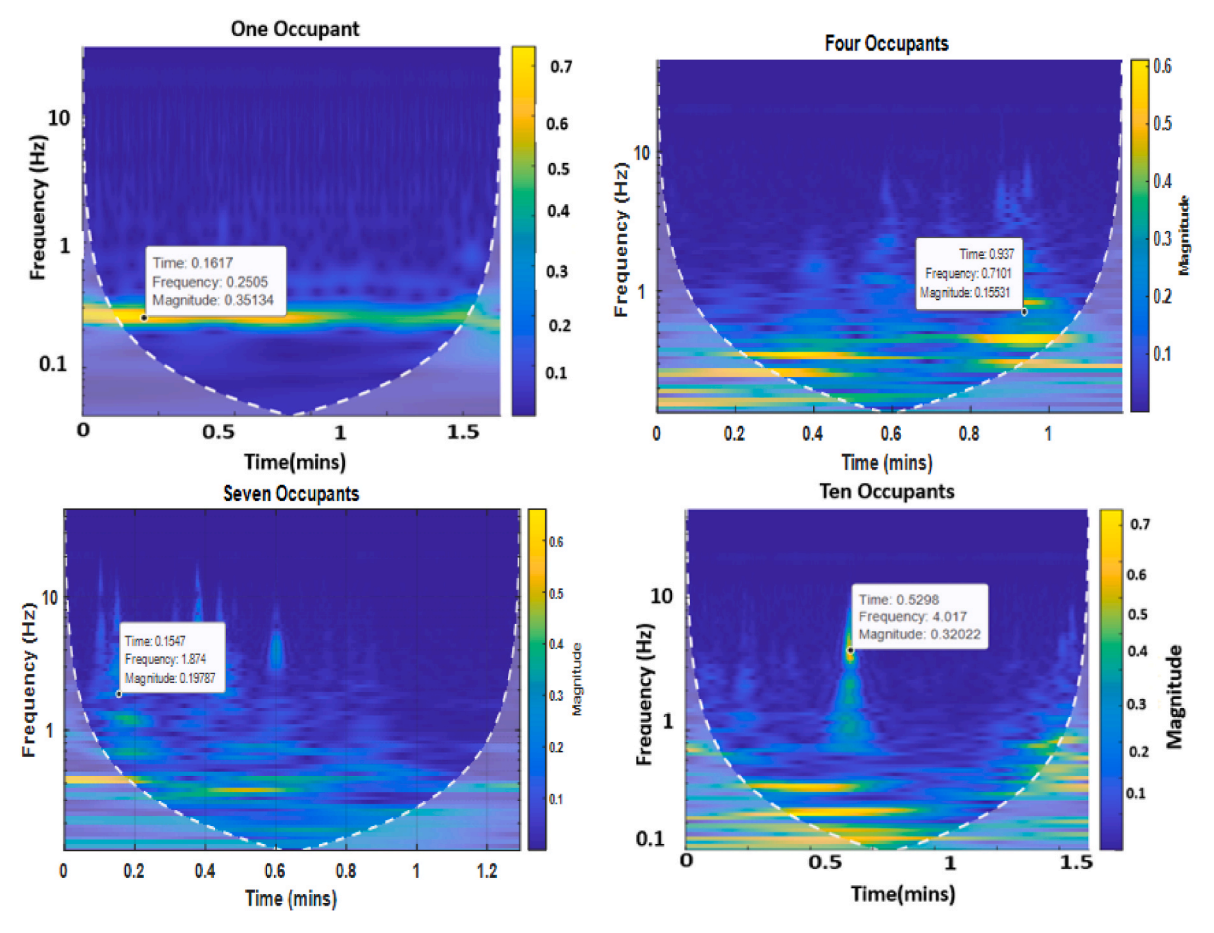
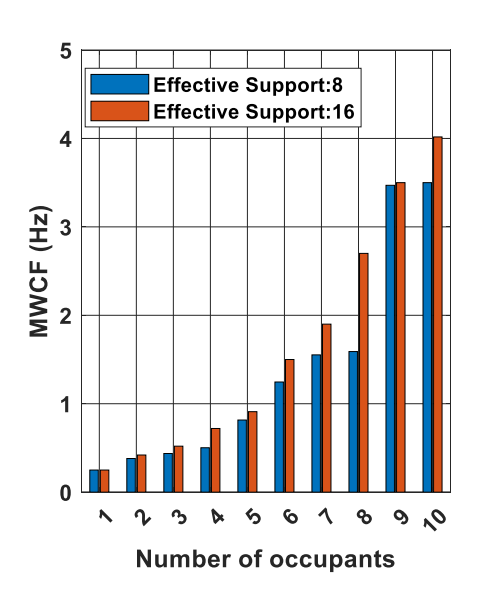


Fig. 7. Wavelet scalogram of the subsampled, lowpass filtered baseband signal from experimental data for (a) one occupant, (b) four occupants, (c) seven occupants, and (d) ten occupants. This wavelet transform was performed with the Morlet wavelet with effective support of 16 and a 60-s window of data. The spectrum has more variation in both time and frequency as the number of occupants increases, and the frequency associated with the maximum value in time-frequency space (MWCF) also increases with the number of occupants with values of 0.23Hz for one occupant, 0.46Hz for 4 occupants, 0.58Hz for 7 occupants, and 1.2Hz for 10 occupants.



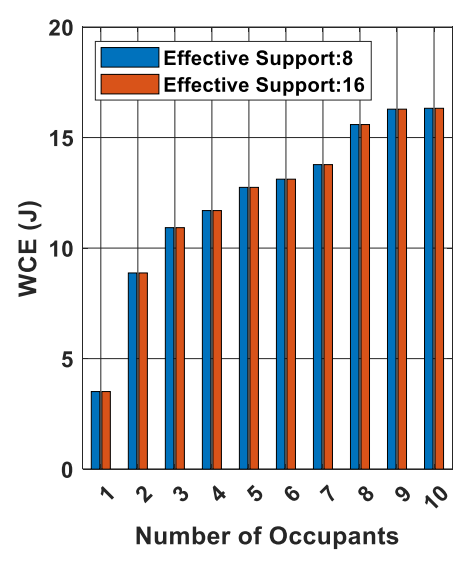


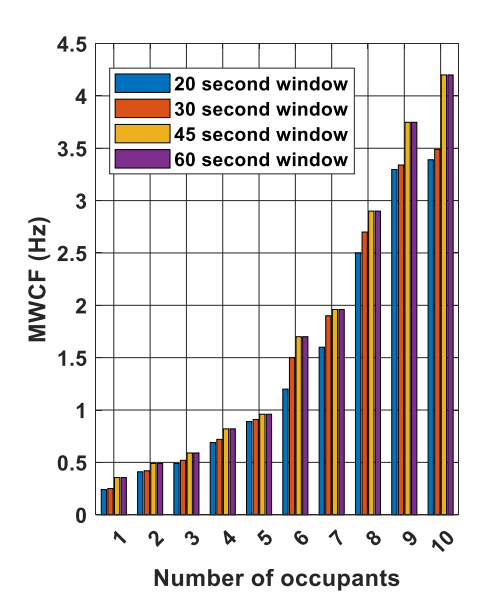
Fig. 8. (left) Relationship between the MWCF of the segmented portion of the signal and the number of occupants in a room with wavelet effective support of 8 and 16. With the increase in the number of occupants there is a more proportional trend in frequency when the effective support function is set to 16 than when it is 8. (right) Relationship between the WCE of the segmented portion of the signal and the number of occupants in a room with wavelet effective support of 8 and 16. No significant difference in this parameter is noted with varied effective support.

4. Results and discussion

4.1. Wavelet effective support

Fig. 6 illustrates the spectra of the linearly demodulated signals for one through ten occupants and Fig. 7 shows the wavelet scalograms of

the linearly demodulated signals for one, four, seven, and ten occupants. As the number of occupants increases, signals include more frequency content above and below breathing frequencies. When there are multiple subjects present in the radar field of view, the radar receives multiple breathing patterns and the mixer non-linearity results in intermodulation products. The constructive and destructive interference of these



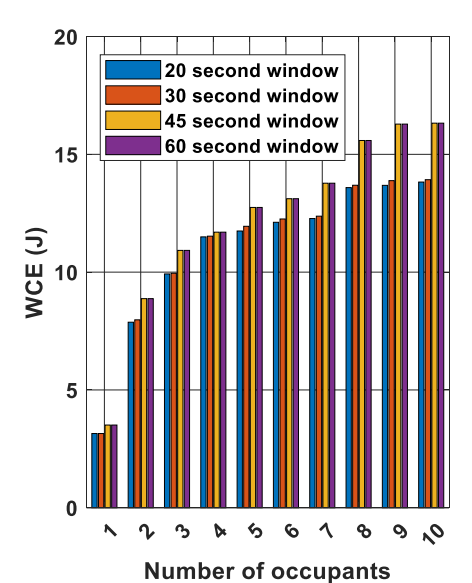


Fig. 9. Relationship between the MWCF (left) and WCE (right) and occupant count with window length set at 20 s, 30 s, 45 s, and 60 s. The relationship between the MWCF and the number of occupants is more linear with 45 and 60 s windows than it is with 20 and 30 s windows but is monotonically increasing in all cases. The relationship between WCE shows greater differentiation between 6 and 9 occupants with 45 and 60 s windows than with 20 and 30 s windows but is also monotonically increasing in all cases.

intermodulation products at different frequencies being effectively summed makes the signals appear aperiodic [38].

The MWCF and the WCE of the segmented 60s window of data was calculated for one to ten occupants, and as the number of participants in the room increased, the MWCF and WCE also increased.

The impact of wavelet effective support was investigated by increasing the effective support from 8 ([-4 4]) to 16 ([-8 8]). When the effective support of the wavelet broadens, the MWCF varies more consistently with the number of occupants, but the WCE does not seem to be significantly impacted by effective support. This increase in variation of the MWCF likely occurs due to Morlet wavelet's center frequency and spectrum breadth increasing with broader effective support. Fig. 8 illustrates the trend between the output parameters and the number of occupants with effective supports of 8 and of 16. With an increase in the number of occupants, there is an increase in the MWCF and the WCE of the segmented signal, regardless of effective support. The increase in the effective support provides better correlation between the MWCF and the number of occupants but does not have a notable impact on the relationship between the WCE and the number of occupants. Effective supports broader than 16 were tested and showed no noticeable change from the results with an effective support of 16 for

this data.

4.2. Window length

Additionally, we explored the dependence of the output on the window length of the analyzed signal [59]. There is no analytical equation to calculate the optimum window length because this algorithm extracts MWCF and WCE using numerical methods [59], thus we experimentally investigated the reliability of the relationship between MWCF and WCE and the number of occupants with different window sizes. We used variable sliding windows for the segmented portion of the signal to evaluate the relationship between each of MWCF and WCE and the number of occupants. We found that with the change of window length, both MWCF and WCE change in some cases; this is expected because their values depend on the signal pattern within the window. However, there is still a monotonically increasing relationship between each of MWCF and WCE and the number of occupants with all tested window lengths. Fig. 9 illustrates the relationship between both MWCF and WCE and the number of occupants for window lengths from 20 to 60 s. We observed that once the window size crosses above 40 s, the MWCF and WCE perfectly match the full 60-s periodic segmented

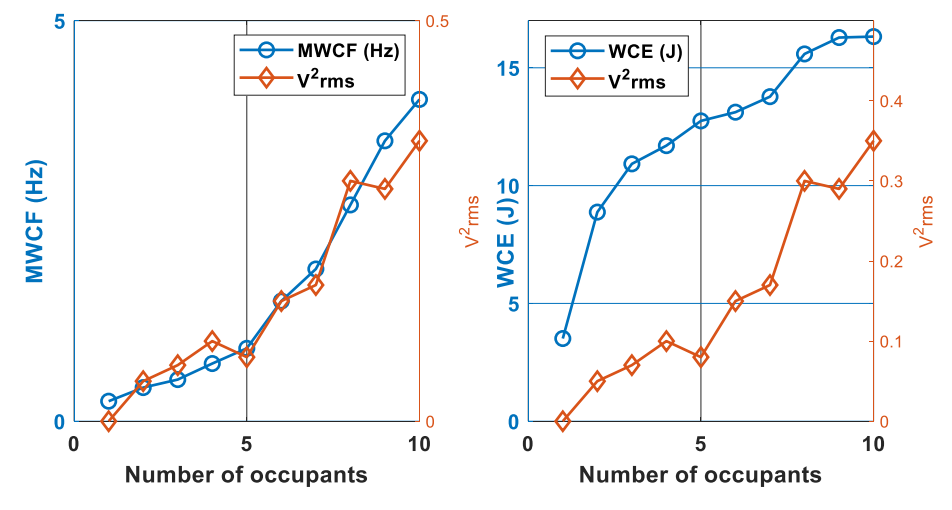


Fig. 10. Comparative analysis between MWCF and received signal strength (RSS) with the number of occupants (left) and between WCE and received signal strength (RSS) with the number of occupants (right). The MWCF and WCE correlate more closely with the number of occupants than RSS does, and the MWCF and WCE are monotonically increasing with the number of occupants while the RSS is not.

window. Regardless of window size, there exists a strong relationship between the MWCF and WCE and the number of occupants. Although the optimal value is at least 45 s for this data set, the algorithms work well with a 20-s window as well, thus windows between 20 and 45 s can be used for occupant estimation if a segment greater than or equal to 45 s is not available.

4.3. Comparative analysis with the proposed method with methods in existing literature

To test how this method compares with previous work, we compared our proposed wavelet-based method results with the received signal strength (RSS) method [48]. The RSS was calculated as the root mean square of the linearly demodulated segmented signals [48]. Fig. 10 shows the comparative graph between the variation of the MWCF, WCE, and RSS vs the number of occupants. Because the MWCF and WCE are monotonically increasing with occupant count, and RSS is not, the wavelet-based methods offer a more robust approach for occupant count estimation. Irregularity in the RSS signal can be caused by some subjects being obscured by others, resulting in a smaller effective radar cross-section [48] and by sensitivity to antenna placement; if the antenna is more focused on a subset of occupants, or if some occupants are closer to the antenna than others, the signal from those occupants can dominate the received signal. On the other hand, varying signal strength from multiple occupants has less impact on wavelet time-frequency mapping, making wavelet coefficients, and therefore WMCF and WCE, less sensitive to individual occupant placement.

4.4. Limitations of this work

One limitation in radar-based occupancy detection is that motion from large body movements obscures the respiration signals, which are required for this approach to estimating occupant count. In this work, we have mitigated this concern by segmenting the signal to eliminate portions that have large body motion [58,59]. This means that this algorithm only estimates the number of occupants while occupants are all stationary. Since the minimum required window size was determined to be only 20–40 s, it is feasible that such data segments, when occupants are mostly stationary, will be available in realistic occupant scenarios. This approach could be useful in conjunction with other occupancy sensors that do not accurately count stationary occupants, or those that accumulate errors (such as doorway sensors) and could use periodic corrections when all occupants are stationary.

Additionally, although low-cost, accurate occupant count sensing is a missing element in demand-controlled ventilation, it is not trivial to control the building environment based on the number of occupants. Because fresh airflow is supplied via a network of ventilation ducts, it can take time to supply fresh air and reduce CO2 and pollutants, even with real-time occupancy data. Several authors have developed algorithms that use occupancy data to predict future occupancy profiles, so the ventilation needs can be forecast [60–63]. Furthermore, occupant activity levels and metabolism can impact required ventilation, and risk of respiratory infection may further inform ventilation rates [64–66].

5. Conclusion

This work presented theoretical background, and comprehensive simulation and experimental results that demonstrated the potential of using Doppler radar and wavelet-based signal processing techniques for estimating the number of occupants. Extensive simulations and testing, including varying wavelet effective support and Doppler radar data window sizes, confirmed that both MWCF and WCE exhibit a robust, monotonically increasing trend as the number of occupants increases. The strong relationship between the MWCF and WCE determined with these methods and the number of occupants encourages us for further algorithm development. For our future work, we will test these

algorithms in more settings and in less controlled scenarios and establish thresholds to estimate the number of occupants after determining the MWCF and WCE. Testing in additional environments will help determine how to best leverage these two parameters for accurate occupant count. Minimum required window size of 20–45 s may enable near real-time implementation of this approach for DCV and other smart building applications.

Additional information

This research was supported in part by the National Science Foundation (NSF) under grant IIP-1831303. Dr. Boric-Lubecke and Dr. Lubecke hold equity and serve as president and vice-president of Adnoviv, Inc, the company that is the prime awardee of the NSF STTR grant that is supporting this work. The University of Hawaii has granted a license to Adnoviv, Inc, to commercialize Doppler radar technology for occupancy sensing purposes, and owns equity in Adnoviv, Inc.

Dr. Droitcour is employed by Adnoviv Inc and has incentive stock options from the company. Dr. Yavari was formerly employed by Adnoviv, Inc.

CRediT authorship contribution statement

Shekh M.M. Islam: Writing – original draft, Visualization, Validation, Software, Methodology, Formal analysis, Conceptualization. Amy Droitcour: Writing – review & editing, Writing – original draft, Visualization, Validation, Supervision, Software, Methodology, Investigation, Formal analysis. Ehsan Yavari: Methodology, Investigation, Data curation. Victor M. Lubecke: Supervision, Project administration, Conceptualization. Olga Boric-Lubecke: Writing – review & editing, Supervision, Resources, Project administration, Investigation, Funding acquisition, Conceptualization.

Declaration of competing interest

The authors declare the following financial interests/personal relationships which may be considered as potential competing interests: Amy Droitcour reports financial support was provided by National Science Foundation. Ehsan Yavari reports financial support was provided by National Science Foundation. Victor M. Lubecke reports financial support was provided by National Science Foundation. Olga Boric-Lubecke reports financial support was provided by National Science Foundation. Amy Droitcour reports a relationship with Adnoviv, Inc. that includes: employment and equity or stocks. Victor M. Lubecke reports a relationship with Adnoviv, Inc. that includes board membership and equity or stocks. Olga Boric-Lubecke reports a relationship with Adnoviv, Inc. that includes: board membership and stocks. Amy Droitcour has patent pending to Adnoviv, Inc. Shekh M. M. Islam has a patent pending to Adnoviv, Inc.

This research was supported in part by the National Science Foundation (NSF) under grant IIP-1831303. Dr. Boric-Lubecke and Dr. Lubecke hold equity and serve as president and vice-president of Adnoviv, Inc, the company that is the prime awardee of the NSF STTR grant that is supporting this work. The University of Hawaii has granted a license to Adnoviv, Inc, to commercialize Doppler radar technology for occupancy sensing purposes, and owns equity in Adnoviv, Inc.

Dr. Yavari was formerly employed by Adnoviv, Inc.

Data availability

Data will be made available on request.

Acknowledgment

This work was supported in part by the National Science Foundation (NSF) under grant IIP-1831303.

References

- [1] S. Azimi, W. O'Brien, Fit-for-purpose: measuring occupancy to support commercial building operations: a review, Build. Environ. 212 (Mar. 2022), 108767, https:// doi.org/10.1016/j.buildenv.2022.108767.
- [2] M. Hu, M. Simon, S. Fix, A.A. Vivino, E. Bernat, Exploring a sustainable building's impact on occupant mental health and cognitive function in a virtual environment, Sci. Rep. 11 (1) (Mar. 2021) 5644, https://doi.org/10.1038/s41598-021-85210-9.
- [3] W. Tushar, et al., Internet of things for green building management: disruptive innovations through low-cost sensor technology and artificial intelligence, IEEE Signal Process. Mag. 35 (5) (Sep. 2018) 100–110, https://doi.org/10.1109/ MSP.2018.2842096.
- [4] P. MacNaughton, J. Spengler, J. Vallarino, S. Santanam, U. Satish, J. Allen, Environmental perceptions and health before and after relocation to a green building, Build. Environ. 104 (Aug. 2016) 138–144, https://doi.org/10.1016/j. buildenv.2016.05.011.
- [5] L. Bergefurt, M. Weijs-Perrée, R. Appel-Meulenbroek, T. Arentze, The physical office workplace as a resource for mental health – a systematic scoping review, Build. Environ. 207 (Jan. 2022), 108505, https://doi.org/10.1016/j. buildenv.2021.108505
- [6] A.J. Hoisington, et al., Ten questions concerning the built environment and mental health, Build. Environ. 155 (May 2019) 58–69, https://doi.org/10.1016/j. buildenv.2019.03.036.
- [7] U. Satish, et al., Is CO2 an indoor pollutant? Direct effects of low-to-moderate CO2 concentrations on human decision-making performance, Environ. Health Perspect. 120 (12) (Dec. 2012) 1671–1677, https://doi.org/10.1289/ehp.1104789.
- [8] O. Seppänen, W.J. Fisk, Q.H. Lei, Ventilation and performance in office work, Indoor Air 16 (1) (2006) 28–36.
- [9] N. Ildiri, H. Bazille, Y. Lou, K. Hinkelman, W.A. Gray, W. Zuo, Impact of WELL certification on occupant satisfaction and perceived health, well-being, and productivity: a multi-office pre- versus post-occupancy evaluation, Build. Environ. 224 (Oct. 2022), 109539, https://doi.org/10.1016/j.buildenv.2022.109539.
- [10] J. Kallio, et al., Assessment of perceived indoor environmental quality, stress and productivity based on environmental sensor data and personality categorization, Build. Environ. 175 (May 2020), 106787, https://doi.org/10.1016/j. buildenv.2020.106787.
- [11] S. D'Oca, T. Hong, J. Langevin, The human dimensions of energy use in buildings: a review, Renew. Sustain. Energy Rev. 81 (Jan. 2018) 731–742, https://doi.org/ 10.1016/j.rser.2017.08.019.
- [12] A. Paone, J.-P. Bacher, The impact of building occupant behavior on energy efficiency and methods to influence it: a review of the state of the art, Energies 11 (4) (Apr. 2018) 953, https://doi.org/10.3390/en11040953.
- [13] Z. Chen, C. Jiang, L. Xie, Building occupancy estimation and detection: a review, Energy Build. 169 (Jun. 2018) 260–270, https://doi.org/10.1016/j. enbuild.2018.03.084.
- [14] https://www.eia.gov/consumption/commercial/data/2012/c&e/cfm.php.
- [15] D. Chen, S. Barker, A. Subbaswamy, D. Irwin, P. Shenoy, Non-intrusive occupancy monitoring using smart meters, in: Proceedings of the 5th ACM Workshop on Embedded Systems for Energy-Efficient Buildings, BuildSys'13, Roma, Italy, 2013, pp. 1–8, https://doi.org/10.1145/2528282.2528294.
- [16] S.S. Shrestha, G.M. Maxwell, An Experimental Evaluation of HVAC-Grade Carbon-Dioxide Sensors— Part 3: Humidity, Temperature, and Pressure Sensitivity Test Results, vol. 116, 2010, p. 14.
- [17] S.J. Emmerich, State-of-the-art Review of CO2 Demand-Controlled Ventilation Technology and Application, National Institute of Standards and Technology, Gaithersburg, MD, 2001. NIST IR 6729.
- [18] C. de Bakker, M. Aries, H. Kort, A. Rosemann, Occupancy-based lighting control in open-plan office spaces: a state-of-the-art review, Build. Environ. 112 (Feb. 2017) 308–321, https://doi.org/10.1016/j.buildenv.2016.11.042.
- [19] M. Jacoby, S.Y. Tan, G. Henze, S. Sarkar, A high-fidelity residential building occupancy detection dataset, Sci. Data 8 (1) (Oct. 2021) 280, https://doi.org/ 10.1038/s41597-021-01055-x.
- [20] W.J. Fisk, D.P. Sullivan, D. Faulkner, E. Eliseeva, CO2 monitoring for demand controlled ventilation in commercial buildings, LBNL- 3279E (Mar. 2010), 983161.
- [21] G. Ansanay-Alex, "Estimating occupancy using indoor carbon dioxide concentrations only in an office building: a method and qualitative assessment," Proceedings Of the REHVA World Congress on Energy Efficient, Smart and Health Buildings, pp. 1-8, 2013.
- [22] Junjing Yang, Matthoes Santamouris, Siew Eang Lee, Review of occupancy sensing system and occupancy modelling methodologies for the application in institutional buildings, Energy Build. 121 (June 2016) 344–349.
- [23] F. Fleuret, J. Berclaz, R. Lengagne, P. Fua, Multicamera people tracking with a probabilistic occupancy map, IEEE Trans. Pattern Anal. Mach. Intell. 30 (2) (Feb. 2008) 267–282, https://doi.org/10.1109/TPAMI.2007.1174.
- [24] J.H. Schwee, et al., Room-level occupant counts and environmental quality from heterogeneous sensing modalities in a smart building, Sci. Data 6 (1) (Dec. 2019) 287, https://doi.org/10.1038/s41597-019-0274-4.
- [25] B. Balaji, J. Xu, A. Nwokafor, R. Gupta, Y. Agarwal, Occupancy based HVAC actuation using existing wi-fi infrastructure within commercial buildings, in: Proceedings Of the 11th ACM Conference On Embedded Network Sensor System, 2013, pp. 17–22
- [26] E. Yavari, C. Song, V. Lubecke, O. Boric-Lubecke, Is there anybody in there? Intelligent radar occupancy sensors, IEEE Microwave 15 (2) (Mar. 2014) 57–64, https://doi.org/10.1109/MMM.2013.2296210.
- [27] E. Yavari, H. Jou, V. Lubecke, O. Boric-Lubecke, Doppler radar sensor for occupancy monitoring, in: 2013 IEEE Topical Conference on Power Amplifiers for

- Wireless and Radio Applications, 2013, pp. 145–147, https://doi.org/10.1109/PAWR.2013.6490217. Austin, TX, USA.
- [28] M. Mercuri, I.R. Lorato, Y.-H. Liu, F. Wieringa, C.V. Hoof, T. Torfs, Vital-sign monitoring and spatial tracking of multiple people using a contactless radar-based sensor, Nat Electron 2 (6) (Jun. 2019) 252–262, https://doi.org/10.1038/s41928-019-0258-6
- [29] X. Hui, E.C. Kan, Radio ranging with ultrahigh resolution using a harmonic radio-frequency identification system, Nat Electron 2 (3) (Mar. 2019) 125–131, https://doi.org/10.1038/s41928-019-0219-0.
- [30] K. Shi, et al., A dataset of radar-recorded heart sounds and vital signs including synchronised reference sensor signals, Sci. Data 7 (1) (Dec. 2020) 50, https://doi. org/10.1038/s41597-020-0390-1.
- [31] S. Rahman, D.A. Robertson, Radar micro-Doppler signatures of drones and birds at K-band and W-band, Sci. Rep. 8 (1) (Dec. 2018), 17396, https://doi.org/10.1038/ s41598-018-35880-9
- [32] P. Sharma, X. Hui, J. Zhou, T.B. Conroy, E.C. Kan, Wearable radio-frequency sensing of respiratory rate, respiratory volume, and heart rate, npj Digit. Med. 3 (1) (Dec. 2020) 98, https://doi.org/10.1038/s41746-020-0307-6.
- [33] C. Song, A.D. Droitcour, S.M.M. Islam, A. Whitworth, V.M. Lubecke, O. Boric-Lubecke, Unobtrusive occupancy and vital signs sensing for human building interactive systems, Sci. Rep. 13 (1) (Jan. 2023) 954, https://doi.org/10.1038/ s41598-023-27425-6.
- [34] O. Rioul, M. Vetterli, Wavelets and signal processing, IEEE Signal Process. Mag. 8 (4) (Oct. 1991) 14–38, https://doi.org/10.1109/79.91217.
- [35] I. Hossain, Z. Moussavi, An overview of heart-noise reduction of lung sound using wavelet transform based filter, in: Proceedings of the 25th Annual International Conference of the IEEE Engineering in Medicine and Biology Society (IEEE Cat. No.03CH37439), Cancun, Mexico, 2003, pp. 458–461, https://doi.org/10.1109/ IEMBS.2003.1279719.
- [36] Jung Jun Lee, Sang Min Lee, Kim In Young, Hong Ki Min, Seung Hong Hong, Comparison between short time Fourier and wavelet transform for feature extraction of heart sound, in: Proceedings Of IEEE. IEEE Region 10 Conference. TENCON 99. "Multimedia Technology For Asia-Pacific Information Infrastructure" (Cat. No.99CH37030), vol. 2, Cheju Island, South Korea, 1999, pp. 1547–1550, https://doi.org/10.1109/TENCON.1999.818731.
- [37] M. Yashita, N. Hamada, Time-frequency masking method using wavelet transform for BSS problem, in: TENCON 2006 - 2006 IEEE Region 10 Conference, 2006, pp. 1–4, https://doi.org/10.1109/TENCON.2006.343856. Hong Kong, China.
- [38] B.Y. Su, K.C. Ho, M.J. Rantz, M. Skubic, Doppler radar fall activity detection using the wavelet transform, IEEE Trans. Biomed. Eng. 62 (3) (Mar. 2015) 865–875, https://doi.org/10.1109/TBME.2014.2367038.
- [39] M. Li, J. Lin, Wavelet-transform-based data-length-variation technique for fast heart rate detection using 5.8-GHz CW Doppler radar, IEEE Trans. Microw. Theor. Tech. 66 (1) (Jan. 2018) 568–576, https://doi.org/10.1109/TMTT.2017.2730182.
- [40] X. Hu, T. Jin, Short-range vital signs sensing based on EEMD and CWT using IR-UWB radar, Sensors 16 (12) (Nov. 2016) 2025, https://doi.org/10.3390/s16122025
- [41] M. Georgescu, I. Mezic, Estimating occupancy states from building temperature data using wavelet analysis, in: 13th Conference Of International Building Performance Simulation Association", August 26-28, 2013, pp. 1459–1466. Chambery, France.
- [42] Y. Zhou, et al., A novel model based on multi-grained cascade forests with wavelet denoising for indoor occupancy estimation, Build. Environ. 167 (Jan. 2020), 106461, https://doi.org/10.1016/j.buildenv.2019.106461.
- [43] J.C. Lin, Microwave sensing of physiological movement and volume change: a review, Bioelectromagnetics 13 (6) (1992) 557–565, https://doi.org/10.1002/ bem.2250130610.
- [44] A. Droitcour, V. Lubecke, Jenshan Lin, O. Boric-Lubecke, A microwave radio for Doppler radar sensing of vital signs, in: 2001 IEEE MTT-S International Microwave Symposium Digest (Cat. No.01CH37157), vol. 1, 2001, pp. 175–178, https://doi. org/10.1109/MWSYM.2001.966866. Phoenix, AZ, USA.
- [45] S.M.M. Islam, E. Yavari, A. Rahman, V.M. Lubecke, O. Boric-Lubecke, Multiple subject respiratory pattern recognition and estimation of direction of arrival using phase-comparison monopulse radar, in: 2019 IEEE Radio and Wireless Symposium (RWS), 2019, pp. 1–4, https://doi.org/10.1109/RWS.2019.8714272. Orlando, FL, IISA
- [46] A. Mishra, W. McDonnell, J. Wang, D. Rodriguez, C. Li, Intermodulation-based nonlinear smart health sensing of human vital signs and location, IEEE Access 7 (2019) 158284–158295, https://doi.org/10.1109/ACCESS.2019.2950347.
- [47] S.M.M. Islam, A. Rahman, Narayana Prasad, O. Boric-Lubecke, Victor Lubecke, Identity authentication system using support vector machine on radar respiration measurement, in: 93rd ARFTG Microwave Measurement Conference, ARFTG), Boston, MA, USA, 2019.
- [48] E. Yavari, X. Gao, O. Boric-Lubecke, Subject count estimation by using Doppler radar occupancy sensor, in: 2018 40th Annual International Conference of the IEEE Engineering in Medicine and Biology Society, EMBC), Honolulu, HI, 2018, pp. 4428–4431, https://doi.org/10.1109/EMBC.2018.8513388.
- [49] J. Carr, Chapter 16 Radio Receiver Basics, the Technician's EMI Handbook, 2000, pp. 163–195.
- [50] L.P.A. Arts, L. Egon, Broek van den, The fast continuous wavelet transformation (fCWT) for real-time, high-quality, noise-resistant time-frequency analysis, Nat Comput Sci 2 (1) (Jan. 2022) 47–58, https://doi.org/10.1038/s43588-021-00183-
- [51] D.-H. Jeong, Y.-D. Kim, I.-U. Song, Y.-A. Chung, J. Jeong, Wavelet energy and wavelet coherence as EEG biomarkers for the diagnosis of Parkinson's disease-

- related dementia and alzheimer's disease, Entropy 18 (1) (Dec. 2015) 8, https://doi.org/10.3390/e18010008.
- [52] L. Guo, D. Rivero, J.A. Seoane, A. Pazos, Classification of EEG signals using relative wavelet energy and artificial neural networks, in: Proceedings of the First ACM/ SIGEVO Summit on Genetic and Evolutionary Computation - GEC '09, 2009, p. 177, https://doi.org/10.1145/1543834.1543860. Shanghai, China.
- [53] H. Heidari Bafroui, A. Ohadi, Application of wavelet energy and Shannon entropy for feature extraction in gearbox fault detection under varying speed conditions, Neurocomputing 133 (Jun. 2014) 437–445, https://doi.org/10.1016/j. neucom.2013.12.018.
- [54] S.M.M. Islam, E. Yavari, A. Rahman, V.M. Lubecke, O. Boric-Lubecke, Separation of respiratory signatures for multiple subjects using independent component analysis with the JADE algorithm, in: 2018 40th Annual International Conference Of the IEEE Engineering In Medicine And Biology Society, EMBC), Honolulu, HI, 2018, pp. 1234–1237, https://doi.org/10.1109/EMBC.2018.8512583.
- [55] A. Singh, et al., Data-based quadrature imbalance compensation for a CW Doppler radar system, IEEE Trans. Microw. Theor. Tech. 61 (4) (April 2013) 1718–1724.
- [56] B.-K. Park, O. Boric-Lubecke, V.M. Lubecke, Arctangent demodulation with DC offset compensation in quadrature Doppler radar receiver systems, IEEE Trans. Microw. Theor. Tech. 55 (5) (May 2007) 1073–1079, https://doi.org/10.1109/TMTT.2007.80552.
- [57] G. Funes, Á. Fernández, D.G. Pérez, L. Zunino, E. Serrano, Estimating the optimal sampling rate using wavelet transform: an application to optical turbulence, Opt Express 21 (13) (Jul. 2013), 15230, https://doi.org/10.1364/OE.21.015230.
- [58] C. Li, J. Lin, "Random body movement cancellation in Doppler radar vital sign detection", IEEE Trans. Microw. Theor. Tech., vol. 56, pp. 3143-3152, doi: 10.1109/TMTT.2008.2007139.

- [59] C. Gu, G. Wang, T. Inoue, C. Li, Doppler radar vital sign detection with random body movement cancellation based on adaptive phase compensation, in: Proceedings of the 2013 IEEE MTT-S International Microwave Symposium Digest (MTT), 2013, https://doi.org/10.1109/MWSYM.2013.669761. Seattle, WA, USA, 2-7 June.
- [60] C. Zhuang, R. Choudhary, A. Mavrogianni, Probabilistic occupancy forecasting for risk-aware optimal ventilation through autoencoder Bayesian deep neural networks, Build. Environ. 219 (Jul. 2022), 109207, https://doi.org/10.1016/j. buildenv.2022.109207.
- [61] Y. Jin, D. Yan, A. Chong, B. Dong, J. An, Building occupancy forecasting: a systematical and critical review, Energy Build. 251 (Nov. 2021), 111345, https://doi.org/10.1016/j.enbuild.2021.111345.
- [62] J. Wang, J. Huang, Z. Feng, S.-J. Cao, F. Haghighat, Occupant-density-detection based energy efficient ventilation system: prevention of infection transmission, Energy Build. 240 (Jun. 2021), 110883, https://doi.org/10.1016/j. enbuild.2021.110883.
- [63] Z. Deng, Q. Chen, Reinforcement learning of occupant behavior model for cross-building transfer learning to various HVAC control systems, Energy Build. 238 (May 2021), 110860, https://doi.org/10.1016/j.enbuild.2021.110860.
- [64] J. Kurnitski, et al., Respiratory infection risk-based ventilation design method, Build. Environ. 206 (Dec. 2021), 108387, https://doi.org/10.1016/j. buildenv.2021.108387.
- [65] S. Zhang, Z. Ai, Z. Lin, Occupancy-aided ventilation for both airborne infection risk control and work productivity, Build. Environ. 188 (Jan. 2021), 107506, https://doi.org/10.1016/j.buildenv.2020.107506.
- [66] B. Li, W. Cai, A novel CO2-based demand-controlled ventilation strategy to limit the spread of COVID-19 in the indoor environment, Build. Environ. 219 (Jul. 2022), 109232, https://doi.org/10.1016/j.buildenv.2022.109232.